

Casein Kinase 1 δ/ϵ Inhibitor PF-5006739 Attenuates Opioid Drug-Seeking Behavior

Travis T. Wager,^{*,†} Ramalakshmi Y. Chandrasekaran,[‡] Jenifer Bradley,[‡] David Rubitski,[†] Helen Berke,[‡] Scot Mente,[†] Todd Butler,[‡] Angela Doran,[‡] Cheng Chang,[‡] Katherine Fisher,[†] John Knafels,[‡] Shenping Liu,[‡] Jeff Ohren,[‡] Michael Marconi,[†] George DeMarco,[†] Blossom Sneed,[‡] Kevin Walton,[§] David Horton,[‡] Amy Rosado,[‡] and Andy Mead[‡]

[†]Pfizer Worldwide Research and Development, 610 Main Street, Cambridge, Massachusetts 02139, United States

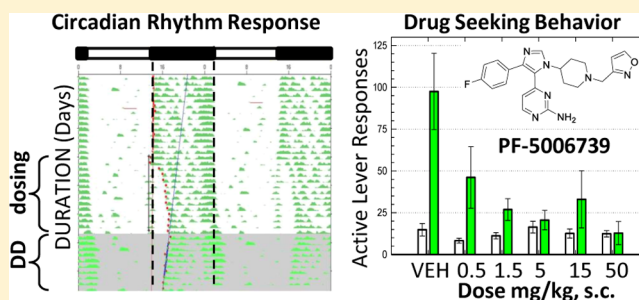
[‡]Pfizer Worldwide Research and Development, Eastern Point Road, Groton, Connecticut 06340, United States

[§]Division of Pharmacotherapies and Medical Consequences of Drug Abuse, National Institute on Drug Abuse, NIH, Rockville, Maryland 20852, United States

Supporting Information

ABSTRACT: Casein kinase 1 delta (CK1 δ) and casein kinase 1 epsilon (CK1 ϵ) inhibitors are potential therapeutic agents for a range of psychiatric disorders. The feasibility of developing a CNS kinase inhibitor has been limited by an inability to identify safe brain-penetrant compounds with high kinome selectivity. Guided by structure-based drug design, potent and selective CK1 δ/ϵ inhibitors have now been identified that address this gap, through the design and synthesis of novel 4-[4-(4-fluorophenyl)-1-(piperidin-4-yl)-1H-imidazol-5-yl]pyrimidin-2-amine derivatives. PF-5006739 (**6**) possesses a desirable profile, with low nanomolar in vitro potency for CK1 δ/ϵ (IC₅₀ = 3.9 and 17.0 nM, respectively) and high kinome selectivity. In vivo, **6** demonstrated robust centrally mediated circadian rhythm phase-delaying effects in both nocturnal and diurnal animal models. Further, **6** dose-dependently attenuated opioid drug-seeking behavior in a rodent operant reinstatement model in animals trained to self-administer fentanyl. Collectively, our data supports further development of **6** as a promising candidate to test the hypothesis of CK1 δ/ϵ inhibition in treating multiple indications in the clinic.

KEYWORDS: Casein kinase 1, CK1 δ , CK1 ϵ , PF-5006739, dual inhibitor, circadian rhythm, phase-delaying, opioid reinstatement, drug addiction



The global burden of disease attributable to opioid dependency increased 74% between 1990 and 2010, which represents a significant epidemic.¹ Opioid dependence accounts for nearly half the estimated 20 million disability-adjusted life years for illicit drug use in 2010, in part due to the early onset of opioid drug abuse (range, 15–24 years old).¹ In 2010, the global prevalence estimate for opioid dependence was over 15 million, and more than half of the 78 000 deaths due to illicit drugs were attributable to opioid dependence.¹ Current strategies to reduce disease burden rely on delivery of medication assisted treatment (methadone, buprenorphine), as well as needle and syringe exchange programs. Given the continued rise in opioid dependency, there clearly remains an urgent need to develop new medicines that can be used to treat addiction and prevent relapse.

Casein kinase 1 delta (CK1 δ) and casein kinase 1 epsilon (CK1 ϵ) are closely related Ser-Thr protein kinases. Mutations and pharmacologic manipulations of each kinase can dramatically alter the circadian period, indicating that they serve as key regulators of the central clock in the supra-

chiasmatic nucleus (SCN).^{2–8} In addition, CK1 δ and ϵ have been linked to the development of drug addictions through the modulation of PERIOD proteins (PER1–3) and dopamine- and cAMP-regulated neuronal phosphoprotein (DARPP-32).^{9–15} Period 1 (PER1) mutants did not sensitize or develop conditioned place preference (CPP) to cocaine, while PER2 mutants showed hypersensitization and strong CPP to cocaine.¹⁰ In addition, PER2 mutants exhibited a 3-fold higher alcohol intake compared to WT, which was suggested to arise from increased glutamate signaling;¹¹ this is reflective of the situation in humans, where PER2 gene variations have been associated with increased alcohol consumption.¹¹ The CK1 δ/ϵ inhibitor compound PF-670462 (**1**) has been shown to prevent relapse-like drinking in rat, an effect which may be due to compound modulation of PER2 within the mesocorticolimbic dopamine system.¹² Both CK1 δ/ϵ isoforms are expressed in the

Received: September 2, 2014

Revised: October 8, 2014

Published: October 9, 2014

Table 1. Summary of in Vitro CK1 δ and CK1 ϵ Inhibitor Activity

Compound	R	CNS MPO	Enzyme CK1 δ IC ₅₀ [nM] ^a	Enzyme CK1 ϵ IC ₅₀ [nM] ^a	WCA CK1 δ EC ₅₀ [nM] ^b	WCA CK1 ϵ EC ₅₀ [nM] ^b	WC ϵ/δ
1	--	4.7	10.4	50.3	36.2	195.0	5.4
2	--	4.2	3.2	12.4	12.4	97.1	7.8
3		4.6	28.5	138.3	133.6	855.3	6.3
4		4.7	32.3	134.4	131.2	911.0	6.9
5		4.7	21.6	106.0	151.7	859.3	5.7
6		4.7	3.9	17.0	15.2	83.0	5.4
7		4.3	7.4	34.3	32.1	194.7	6.1

^aHuman CK1 enzyme data reported as a geometric mean of at least 3 determinations. ^bCK1 whole-cell assay (WCA) data reported as a geometric mean of at least 3 determinations. WCA used COS7 (African green monkey kidney fibroblast) cells and measured nuclear translocation of PER3-GFP.

striatum and cortex and have been reported to regulate glutamatergic synaptic signaling on dopaminergic reward pathways implicated in drug addiction, which may also explain the increased alcohol intake with the PER2 mouse mutations.^{16–18}

CK1 δ/ϵ may affect the physiological response to drugs of abuse by their regulation of DARPP-32. DARPP-32 is highly expressed in medium spiny neurons of the striatum and is involved in the motoric and rewarding effects of drugs of abuse.^{15–17} Heroin, an opioid agonist, significantly upregulates dopamine D1 receptors and DARPP-32 expression.¹⁹ Activation of D1 receptors increases PKA phosphorylation of DARPP-32 at Thr34, converting DARPP-32 into an inhibitor of protein phosphatase PP-1, which results in an increase in the rewarding properties of drugs of abuse.¹⁹ CK1 δ/ϵ is reported to phosphorylate DARPP-32 at Ser130, which increases the phosphorylation state of Thr34 and thereby amplifies D1 dopamine (cAMP/PKA) signaling through the DARPP-32/PP-1 pathway.¹⁸ This amplified signaling may contribute to opioid addiction. Psychostimulants with abuse liability share the same dopaminergic reward pathways as opioids: acute psychostimulant administration has been shown to increase phosphorylation of DARPP-32 Thr34 and Ser130.¹⁸ CK1 δ/ϵ inhibitor **1** attenuates methamphetamine-induced locomotor activity and inhibits DARPP-32 phosphorylation, suggesting a role for CK1 and DARPP-32 phosphorylation in methamphetamine-induced locomotor activity.²⁰ In contrast, selective genetic deletion or pharmacological inhibition of CK1 ϵ increased the sensitivity to locomotor stimulation by methamphetamine and opioids.²¹ Given the body of literature supporting the role of CK1 δ/ϵ in

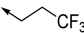
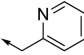
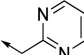
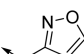
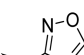
drug addiction, the purpose of the current work was to develop CK1 δ/ϵ inhibitors with improved kinome selectivity and other druglike properties as potential pharmacotherapies for opioid abuse. Reported herein is the discovery of PF-5006739 (**6**), a potent and selective inhibitor of CK1 δ/ϵ .

RESULTS AND DISCUSSION

A high-throughput screening (HTS) approach with a CK1 δ enzyme assay was used to identify a number of potent CK1 inhibitors. One of the first compounds profiled in various ADME assays was **2** (Table 1). In addition to poor in vitro passive permeability, **2** was determined to be a significant P-gp substrate (P-gp ER > 4.5). Subsequent mouse neuropharmacokinetic (neuro-PK) confirmed insignificant CNS exposure ($C_{b,u}/C_{p,u} < 0.03$). In an effort to identify CNS druglike molecules, we utilized structure-based drug design (SBDD) and traditional structure–activity relationships (SAR). This effort yielded **1**, an inhibitor of CK1 δ/ϵ , which we have previously reported.^{3,8,22} Compound **1** provided a major improvement over the HTS lead compound, as it was devoid of P-gp liability and showed improved brain penetration (Table 1). In whole cells transiently expressing CK1 δ or CK1 ϵ and mPER3 GFP, this compound caused a concentration-related redistribution of nuclear versus cytoplasmic PER and, when dosed in mice, produced robust phase delays and entrainment.^{8,23} Compound **1** exhibited high human liver microsomal (HLM) clearance (129 $\mu\text{L}/\text{min}/\text{mg}$), however, resulting in a $t_{1/2}$ of less than 30 min; this prevented further development.

Design of an improved agent was aided by the identification of several structural scaffolds via HTS screening, and structural

Table 2. Summary of ADME Properties

Compound	R	HLM ^a	P_{app} ^b	P-gp ^c	$cC_{max,b,u}$ [nM] ^d	$C_{max,b,u}$ [nM] ^e
1	--	129.5	26.4	1.1	77	72
2	--	16.2	1.6	>4.5	273	12
3		13.1	20.3	1.9	79.7	--
4		18.7	16.8	3.1	36.4	--
5		<9.7	13.5	9.8	53.3	--
6		18.0	22.2	3.2	69	117
7		17.8	15.4	3.5	197	--

^aHuman liver microsomal clearance ($\mu\text{L}/\text{min}/\text{mg}$). ^bPassive permeability ($\text{AB} \times 10^{-6} \text{ cm}/\text{sec}$). ^cMDR1 efflux ratio (BA/AB). ^d $cC_{max,b,u}$ was estimated using the method described by Mente et al.;²⁶ values have been normalized to a dose of 10 mg/kg. ^e $C_{max,b,u}$ values are reported as maximum free drug concentration in brain normalized to a dose of 10 mg/kg.

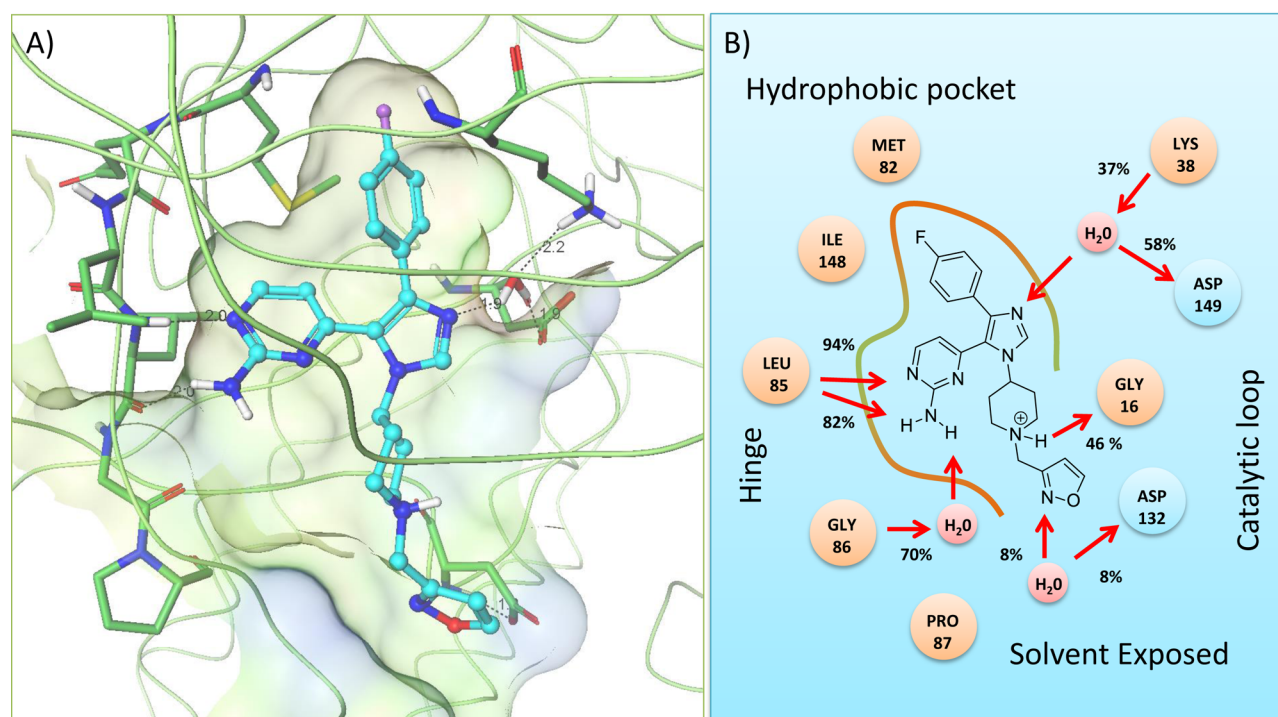


Figure 1. (A) Crystal structure of compound 6 (carbon atoms in cyan, nitrogen in blue, oxygen in red, and fluorine in purple) binding in CK1 δ (backbone diagram) with surface representation. Two-point hinge binding of the aminopyridine core of 6 was observed with hinge residue Leu85. The hydrophobic spine pocket located just inside of the Met82 gatekeeper is optimally occupied by the *p*-fluorophenyl ring of 6. The nitrogen of the imidazole interacts with the catalytic Lys38 through a water molecule. (B) Two-dimensional representation of the crystal structure and molecular dynamics simulated ligand-water-protein interactions. Molecular dynamics protein-ligand simulation interaction fractions are reported in percent of time that interactions were observed during simulation time.

elucidation of their cocrystals with CK1 δ .²² Examination of the cocrystal structure of 1 yielded key insights into how these molecules interact with the protein: (1) the *p*-fluoro phenyl moiety sat within the medium-sized lipophilic selectivity pocket, (2) a key water-mediated interaction existed between

the free imidazole nitrogen and the conserved Lys38, and (3) the aminopyrimidine exhibited a two-point binding interaction with the hinge backbone. These interactions appeared optimal and thus were maintained throughout the SAR effort. The solvent-exposed area appeared to be an ideal region to

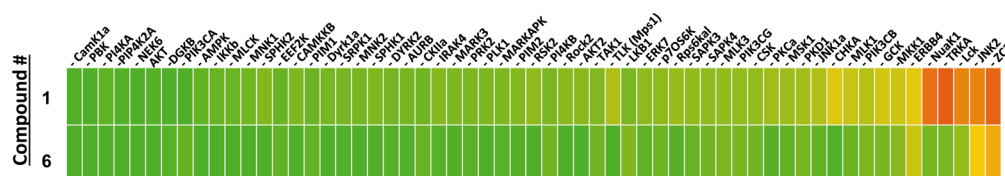


Figure 2. Percent inhibition at 1 μM versus promiscuity panel. Heat map colors continuum: green, 0% inhibition; yellow, 50% inhibition; red, 100% inhibition. IC_{50} determinations were made for compound 6 for the two targets with inhibition > 50% at 1 μM : JNK2 ($\text{IC}_{50} = 6.1 \mu\text{M}$) and ZC3 ($\text{IC}_{50} = 1.5 \mu\text{M}$).

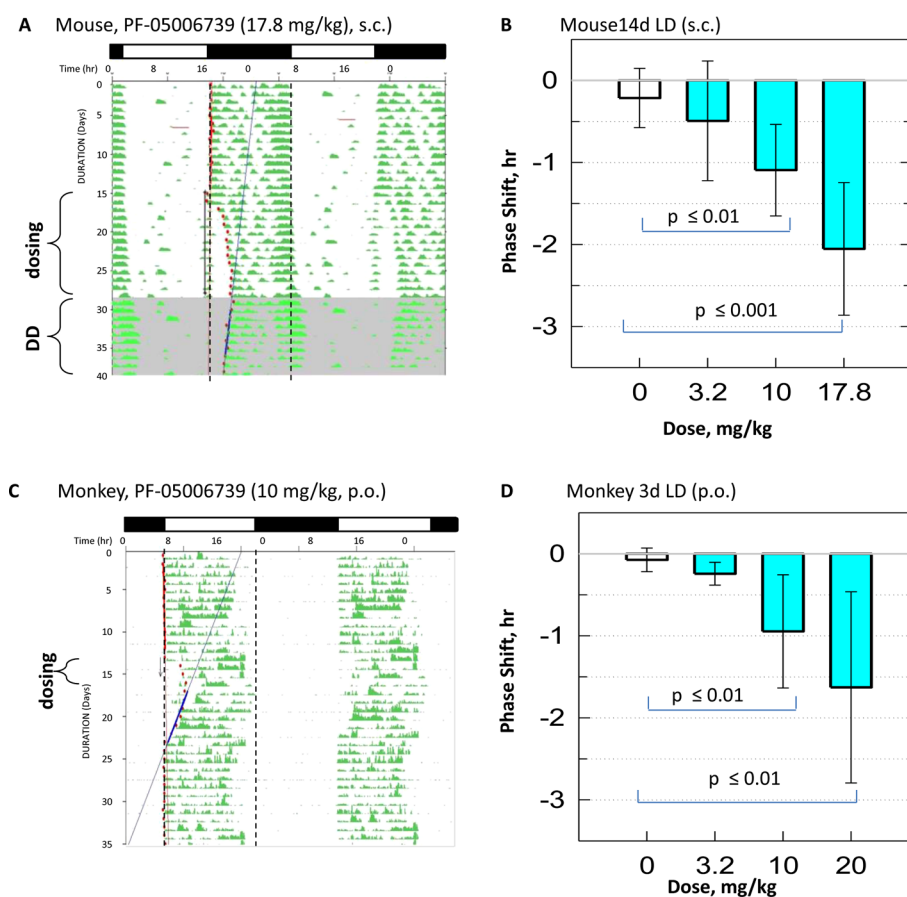


Figure 3. Effects of selective inhibition of $\text{CK1}\delta/\epsilon$ on circadian period of locomotor activity in vivo. (A) Representative body temperature actogram of CS7BL/6J mice treated with 6 under 12 h light (white bar) 12 h dark (black bar), (L:D). (B) Group mouse data revealing dose-dependent phase delay response of compound 6. Lines represent the mean \pm standard error of the mean, significantly phase-delayed after dosing in LD for 14 days with 10 and 17.8 mg/kg dose ($n \geq 6$). There were no significant differences between treatment groups for baseline tau or postdosing tau. (C) Representative actigraphy actogram of Mauritian cynomolgus monkeys treated with 6 under 12:75 h light (white bar), 11:25 h dark (black bar). (D) Group data from the diurnal monkey model data revealing dose-dependent phase delay response of compound 6. Effect of 6 at 3.2, 10, and 20 mg/kg on circadian activity in the monkey model (mean \pm SEM, repeated measure ANOVA with Bonferroni's post hoc test, $n \geq 6$).

interrogate in order to modulate the pharmaceutical properties of the molecules. Therefore, we reinvestigated HTS hit 2, expanding the SAR off the piperidine. Our targeted approach focused on design of molecules with high CNS MPO desirability (>4/6) that maintained a weakly basic site ($\text{pK}_a < 7$) expected to improve solubility and aid in oral bioavailability.^{24,25}

Targeting the solvent-accessible portion of the protein was fruitful, yielding several potent CK1 kinase inhibitors (Table 1) with improved pharmaceutical properties (Table 2). The potency SAR for this series of molecules suggested that 5-membered heterocyclic moieties were optimal: compounds 6 and 7 achieved improved in vitro potency relative to that of 1. Compound 6 was approximately 2-fold more potent than 7 in

the mPER3-GFP whole-cell translocation assay and maintained a whole-cell $\text{CK1}\delta/\text{CK1}\epsilon$ ratio comparable to 1. Analysis of the crystal structure of 6 with $\text{CK1}\delta$ revealed that the protein–ligand interactions were consistent with those previously observed (Figure 1A). Retrospective molecular dynamic simulations between the protein and ligand provided additional insight into the binding affinity of 6 (Figure 1B). Two additional interactions were observed in the molecular dynamic simulation, which do not exist in compound 1: (1) an intermittent water-mediated fractional interaction between the nitrogen of the isoxazole and Asp132, and (2) a robust fractional interaction (46%) between the hydrogen on the basic nitrogen of the piperidine moiety and Gly16.

In addition to excellent physicochemical properties and potency, HLM clearance and passive permeability improved for this set of molecules compared to both **1** and **2** (Table 2). Compound **5** had the lowest HLM clearance of the profiled set ($HLM \leq 9.7$). All of the new compounds had desirable passive permeability, with P_{app} values $\geq 10 \times 10^{-6}$ cm/s. The predicted CNS free brain drug exposure ($cC_{max,b,u}$) at a fixed 10 mg/kg s.c. dose was estimated to be comparable to that exhibited by the CK1 tool compound **1** (Table 2).²⁶ To confirm brain exposure ($C_{max,b,u}$), **1**, **2**, and **6** were evaluated in a neuro-PK study (Table 2). The measured $C_{max,b,u}$ for **2** was significantly lower than estimated free brain exposure, Table 2. The $cC_{max,b,u}$ algorithm does not incorporate P-gp efflux into the calculation, which may account for the over-estimation of brain exposure relative to the measured $C_{max,b,u}$ for **2**.²⁶ Compound **6** demonstrated higher CNS exposure than predicted, with sufficient free drug exposure to cover the whole-cell EC_{50} at a 10 mg/kg s.c. dose. $C_{max,b,u}$ was further used for evaluation of target occupancy (%) as

$$\text{target occupancy} = \frac{C_{b,u}}{C_{b,u} + K_d} \times 100 \quad (1)$$

where the dissociation constant K_d represents in vitro target binding potency. Using the whole-cell EC_{50} as a surrogate for K_d , compound **6** was estimated to have maximum CNS target occupancy of 88% for CK1 δ and 58% for CK1 ϵ , after a 10 mg/kg s.c. dose.

Compound **6** was further evaluated in a kinase selectivity panel, where it demonstrated improved kinome selectivity over the CK1 δ/ϵ tool compound **1** (Figure 2). In a 59-kinase panel, **6** inhibited only 2 targets [JNK2 ($IC_{50} = 6.1 \mu\text{M}$) and ZC3 ($IC_{50} = 1.5 \mu\text{M}$)] at >50% at a drug concentration of 1 μM . Given the fact that **6** was twice as potent at the primary targets (i.e., CK1 δ and CK1 ϵ) as **1**, the fold selectivity over each target was clearly improved.

The next step was to confirm the effect of **6** on circadian rhythm activity in vivo.⁸ Compound **6** produced dose-dependent circadian phase delays in mouse when dosed in a 12 h light and 12 h dark (L:D) paradigm, with a maximum shift of -2.05 h at the 17.8 mg/kg s.c. dose (Figure 3A and B). In a diurnal monkey model, **6** was tested under L:D conditions at 3.2, 10, and 20 mg/kg, oral. Compound **6** induced phase delays in monkey in a dose-dependent manner with a maximum phase shift of -1.6 h (Figure 3C and D). These data suggest that **6** is a robust modulator of circadian rhythm, capable of producing phase delays even in the presence of strong circadian synchronizers such as light. The results from the diurnal monkey model suggested that **6** could have a circadian effect in other diurnal species including humans in nonlab environments.

The in vivo effect of **6** on relapse to substance abuse was evaluated in a rat operant model of fentanyl reinstatement (Figure 4). Analysis of combined cues and fentanyl prime-induced reinstatement revealed a main effect of dose ($F_{(5,45)} = 3.39$; $p < 0.05$), main effect of test ($F_{(1,9)} = 8.34$; $p < 0.05$), and a significant dose by test interaction effect ($F_{(5,45)} = 3.41$; $p < 0.05$). Post hoc comparisons revealed that a significant reinstatement effect was observed in the reinstatement session compared to baseline following administration of vehicle as well as 0.5 and 1.5 mg/kg of **6**. Furthermore, **6** significantly decreased active lever response rates at 1.5, 5, 15, and 50 mg/kg compared to vehicle. Analysis of inactive lever responses

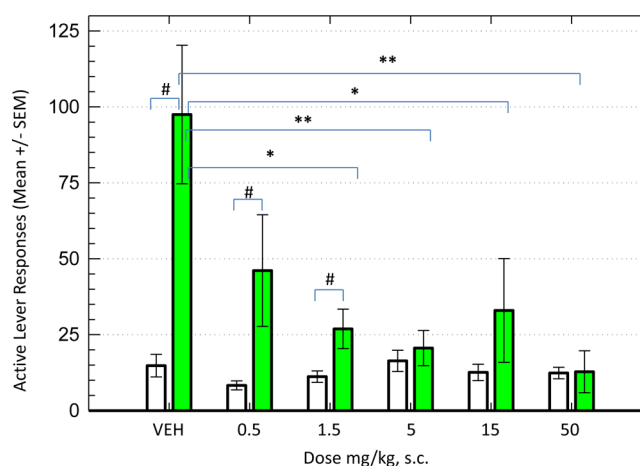


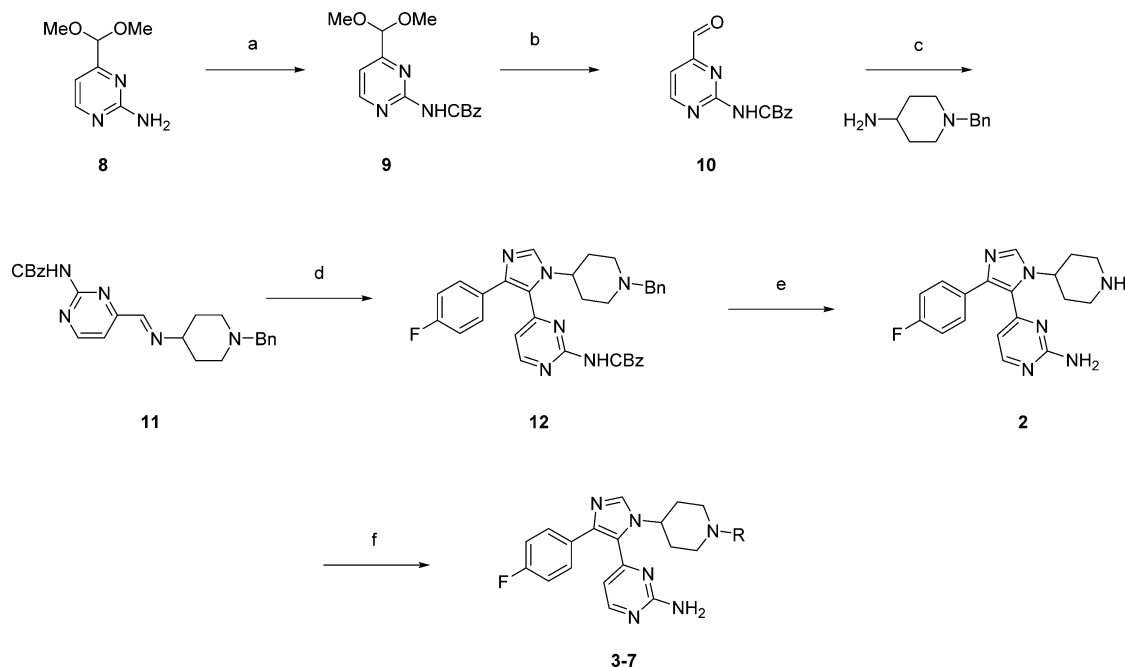
Figure 4. Effects of **6** on reinstatement of fentanyl-seeking behavior in the rat reinstatement model. White bars represent baseline active lever responses and green bars represent active lever responses during the reinstatement test. Data represent mean \pm SEM active lever responses, demonstrating the effect of **6** (0.5–50 mg/kg, s.c., 30 min pretreatment) on combined cue- and fentanyl prime-induced reinstatement, $n = 11$. # $p < 0.05$ compared to active lever responses on baseline conditions; * $p < 0.05$ and ** $p < 0.01$ compared to vehicle active lever response on reinstatement condition.

revealed a main effect of test ($F_{(1,9)} = 18.5$; $p < 0.01$); no main effect of dose or dose by test interaction effect was observed. Post hoc comparisons indicated that a significant decrease in inactive lever responses was observed in the reinstatement session compared to baseline for the 0.5, 15, and 50 mg/kg doses of **6**. Compound **6** dose-dependently prevented reinstatement of fentanyl seeking; analysis of drug concentrations suggests that an average free brain exposure of 5 nM is sufficient to reduce reinstatement by 50%.

CONCLUSION

Commercial development of a kinase inhibitor for CNS indications has yet to be accomplished. Given this fact, we sought to identify a safe brain-penetrant compound with high kinome selectivity and a low projected human efficacious drug concentration (i.e., C_{eff}). Leveraging the knowledge gained from our recent analysis of exploratory toxicology study outcomes, we sought to identify a compound with $C_{eff} \leq 250$ nM (total drug).²⁷

From our extensive compound file and an HTS enzyme assay, the potent CK1 δ/ϵ inhibitor **2** was identified. This HTS hit provided the basis for a set of molecules possessing CNS drug-like properties as defined by CNS MPO desirability ($\geq 4/6$), potency, and ADME properties. Compound **6** exhibited low nanomolar affinity for CK1 δ and ϵ (CK1 δ $IC_{50} = 3.9$ nM; CK1 ϵ $IC_{50} = 17$ nM) in the in vitro purified enzyme assay. Further, whole-cell potency of **6**, the ability to inhibit mPER3-GFP translocation to the nucleus for both CK1 targets, was in the double-digit nanomolar range, with $EC_{50} = 15.2$ and 83 nM, respectively, for CK1 δ and CK1 ϵ . Subsequently, maximum target modulation was evaluated based on both calculated and in vivo observed $C_{max,b,u}$: compound **6** was estimated to have maximum CK1 δ /CK1 ϵ CNS target occupancy of 88% and 58%, respectively, after a 10 mg/kg s.c. dose in mice. Using the CK1 δ whole-cell EC_{50} as a C_{eff} surrogate and human plasma protein binding ($hF_u = 0.46$), we estimated the total drug concentration of **6** to be 47 nM, which is within the C_{eff}

Scheme 1. Synthesis of Compounds 2–7^a

^aReagents and conditions: (a) benzyl chloroformate, pyridine, DCM, $-18\text{ }^{\circ}\text{C}$ to rt (unpurified); (b) aq. HCl (4 M), THF, $40\text{ }^{\circ}\text{C}$ (unpurified); (c) 45% KOH, K_2CO_3 , DCM, $25\text{ }^{\circ}\text{C}$; (d) 1-fluoro-4-[isocyanato(tosyl)methyl]benzene, 20% aq. K_2CO_3 , DCM, rt (62%); (e) $\text{Pd}(\text{OH})_2$, H_2 , MeOH, $40\text{ }^{\circ}\text{C}$ (90%). (f) alkylation or reductive amination.

guidelines of $\leq 250\text{ nM}$ (total drug).²⁷ Ultimately, compound **6** also demonstrated in vivo responses downstream of $\text{CK1}\delta/\epsilon$ inhibition. It dose-dependently modulated circadian rhythm in both nocturnal and diurnal animal models under L:D condition confirming previous reports. More important, the current study demonstrated a connection between $\text{CK1}\delta/\epsilon$ inhibition and prevention of drug-seeking behavior, with compound **6** robustly attenuating fentanyl-seeking behavior under the combined cue and prime conditions at exposure levels that are comparable to its in vitro potency. As the rat reinstatement model of drug relapse possesses high predictive validity for efficacy in substance use disorders,²⁸ this data suggests that $\text{CK1}\delta/\epsilon$ inhibitors warrant further investigation for this therapeutic opportunity.

In summary, compound **6** clearly demonstrated in preclinical settings the “three Pillars of survival” (i.e., exposure at the site of action, target binding, and expression of functional pharmacological activity),²⁹ making it a promising candidate to test the $\text{CK1}\delta/\epsilon$ mechanism for multiple indications in the clinic.

METHODS

Physicochemical Properties and Data Analysis. For the work herein, calculated CNS MPO desirability scores were obtained using the published algorithm,²⁵ and calculated physicochemical properties were obtained using standard commercial packages: Biobyte for clogP calculations; for calculation of TPSA, see Ertl.³⁰ Statistical analyses were carried out using SigmaPlot version 11.0, from Systat Software, Inc. (San Jose, CA, www.sigmaplot.com).

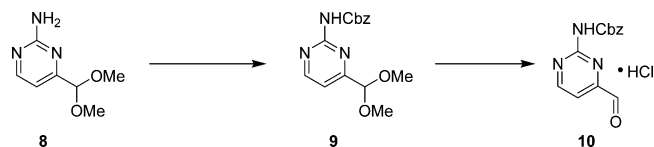
ADME Data. Data on the following in vitro ADME properties were taken from the company files. All assays were performed via reported methods as described previously for the following: (a) passive apparent permeability, P_{app} assay;³¹ (b) P-glycoprotein (P-gp) efflux liability assay;³¹ (c) metabolic stability, expressed as unbound intrinsic clearance ($\text{CL}_{\text{int,u}}$);^{32,33} and (d) plasma protein binding, F_u mouse and human.

Simulation Methods.³⁴ Molecular dynamics setup was started with an initial docking and minimization of the ligand into the PDB of $\text{CK1}\delta$ (4TN6). Following addition of Na^+ ions to neutralize the system and TIP3P waters, the total size of the system was $\sim 48\,000$ atoms. All simulations were performed using the DESMOND simulation package under periodic boundary conditions in a rectangular box at 300 K with the Nosé–Hoover chain thermostat and coupling time constant of 1 ps. All systems were first subjected to a temperature-ramping scheme defined previously,³⁴ followed by 50 ns production runs without any restraints and a time step of 2 fs. Simulation interaction diagrams were calculated using the python script that comes with the MAESTRO installation. All simulations were carried out on a Dell PowerEdge C6220 server with NVIDIA Tesla M2075 GPUs.

Chemistry. The syntheses of casein kinase inhibitors **2–7** are outlined in Scheme 1. The sequence, which was used to prepare material on kilogram scale, began with a mono-Cbz protection of 2-aminopyrimidine **8** via treatment with pyridine and excess benzyl chloroformate.³⁵ After a minimal aqueous workup, the crude product **9** was used as a solution in the benzyl chloride reaction byproduct. This material was treated with aq. HCl to hydrolyze the acetal, affording aldehyde **10**. Attempts to isolate and purify **10** resulted in unacceptably low yields use of the crude acidic solution; however, reaction with 4-amino-1-benzylpiperidine under basic conditions provided a good yield of imine **11** ($\sim 60\%$ over 3 steps from **8**). This imine may be isolated or carried in solution to the next step. Imidazole **12** was formed in 70% yield by cyclization of imine **11** in DCM solution with the tosmic reagent 1-fluoro-4-[isocyanato(tosyl)methyl]benzene in the presence of aq. K_2CO_3 . At this stage, the material was isolated and purified by a combination of chromatography and recrystallization. Removal of the benzyl and Cbz protecting groups via hydrogenolysis, using Pearlman’s catalyst in methanol at $40\text{ }^{\circ}\text{C}$, afforded the penultimate intermediate **2** in 90% yield. This material was used to prepare the various N-substituted piperidine analogues **3–7** either via reductive amination with appropriate aldehydes or by treatment with alkyl or heteroaryl halides in the presence of base.

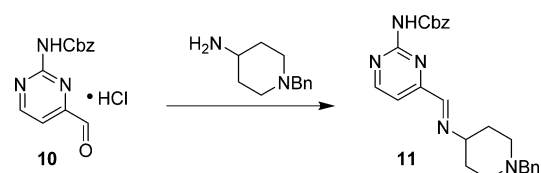
Chemistry Experimental Section. General Information. All solvents and reagents were obtained from commercial sources and were used as received. All reactions were followed by TLC (TLC plates F254, Merck) or LCMS (liquid chromatography–mass spectrometry) analysis. Proton and ^{13}C NMR spectra were obtained using deuterated solvents on a Varian 400 MHz instrument. All proton shifts are reported in δ units (ppm) downfield of TMS (tetramethylsilane) and were measured relative to the signals for chloroform (7.27 ppm) and methanol (3.31 ppm). All ^{13}C shifts are reported in δ units (ppm) relative to the signals for chloroform (77.0 ppm) and methanol (49.1 ppm) with ^1H -decoupled observation. NMR abbreviations are as follows: br, broadened; s, singlet; d, doublet; t, triplet; q, quartet; p, pentuplet; m, multiplet; dd, doublet of doublets; dddd, doublet of doublet of doublets; sept, septuplet; tt, triplet of triplets. Analytical analyses by UPLC were performed on a Waters Acquity system with PDA detection (UV 210 nm) at 45 °C, flow rate 0.5 mL/min, with a gradient of 95/5 buffer/acetonitrile (0–7.55 min), 10/90 buffer/acetonitrile (7.55–7.85 min) using the following columns and buffers: Waters BEH C8 column (2.1 \times 100 mm, 1.7 μm) with 50 mM sodium perchlorate/0.1% phosphoric acid or 10 mM ammonium bicarbonate as buffer; Waters BEH RP C18 column (2.1 \times 100 mm, 1.7 μm) or Waters HSS T3 (2.1 \times 100 mm, 1.8 μm) column with 0.1% methanesulfonic acid buffer. All melting points are uncorrected. Elemental analyses were performed by QTI Development. Mass spectra were recorded on a Micromass ADM atmospheric pressure chemical ionization instrument (MS, APCI). High resolution mass spectra were obtained on an Agilent LC-MS TOF equipped with a Zorbax Eclipse column (50 mm \times 4.6 mm, 1.8 μm XDB-C18) using 0.1% aqueous formic acid as mobile phase A1 and acetonitrile containing 0.1% formic acid as mobile phase B1. Column chromatography was carried out on silica gel 60 (32–60 mesh, 60 Å) or on prepacked Biotage columns. The purities of final compounds 1–7 as measured by UPLC were found to be above 95%.

Preparation of 4-[4-(4-fluorophenyl)-1-(piperidin-4-yl)-1H-imidazol-5-yl]pyrimidin-2-amine (2). *Step 1: Preparation of Benzyl 4-*

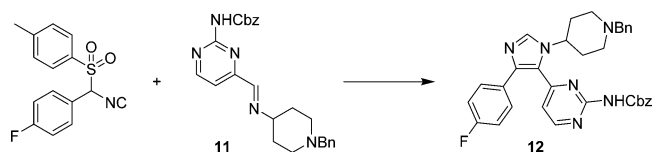


formylpyrimidin-2-ylcarbamate (10). A cold solution of benzyl chloroformate (12.6 kg, 73.90 mol) in DCM (6 L) was added over 6 h to a -18 °C mixture of **8** (1.35 kg, 8.00 mol) and pyridine (800 mL, 9.90 mol) in DCM (30 L), while the reaction temperature was maintained between -18 and -15 °C. The reaction was then allowed to warm to rt overnight; ^1H NMR analysis showed $\sim 65\%$ completion. The mixture was recooled to -18 °C and treated with an additional portion of benzyl chloroformate (1.26 kg, 7.4 mol) in DCM (750 mL). The reaction was warmed to 0 °C, and water (15 L) was added. The layers were separated, and the organic phase was filtered through a pad of silica (4 kg) and washed with 20 L of 20% ethyl acetate in DCM. The filtrate was evaporated to afford 14.2 kg of a $\sim 95:5$ mixture of benzyl 4-(dimethoxymethyl)pyrimidin-2-ylcarbamate (**9**) and starting material in benzyl chloride. Analysis by ^1H NMR showed this mixture to contain $\sim 15\%$ of product by weight. A portion was purified by silica gel chromatography using 50% EtOAc/heptanes to obtain an analytical sample of **9** as a white solid. ^1H NMR (CDCl_3) δ 8.66 (d, $J = 5.1$ Hz, 1H), 8.16 (br s, 1H), 7.31–7.43 (m, 5H), 7.21 (d, $J = 5.1$ Hz, 1H), 5.26 (s, 2H), 5.22 (s, 1H), 3.41 (s, 6H). ^{13}C NMR (CDCl_3) δ 166.9, 159.2, 157.1, 151.3, 135.6, 128.6, 128.4, 128.3, 113.3, 102.3, 67.4, 53.8. HRMS m/z , calcd MH^+ 304.1297, observed 304.1292.

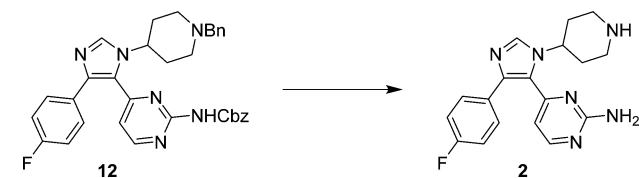
This crude solution of **9** in benzyl chloride (14.2 kg) was diluted with THF (2.5 L), and 4 M HCl (5 L) was added. The mixture was heated to 40 °C overnight and then cooled to 25 °C. The aqueous layer was separated, and the organic layer was re-extracted with 2 M HCl (2 \times 1.1 L). The combined aqueous layers, containing the hydrochloride salt of the title compound **10**, were used directly in the next step without isolation of the aldehyde product.



Step 2: Preparation of Benzyl 4-[[1-(1-Benzylpiperidin-4-yl)imino]methyl]pyrimidin-2-ylcarbamate (11). Aqueous 45% KOH (1.65 L, 19.3 mol) was added slowly to a 5 °C solution of crude aldehyde **10** (≤ 8 mol) in aq. HCl (≤ 24.4 mol from the previous step) while the temperature was maintained below 15 °C. Next, DCM (8 L) and K_2CO_3 (1 kg, 7.2 mol, portion-wise) were added. 4-Amino-1-benzylpiperidine (898 g, 4.72 mol) was added over 4 min at 10 °C, and then the reaction was warmed to 20 °C for 1 h. ^1H NMR analysis showed $\sim 2\%$ aldehyde **10** remaining, with the amine fully consumed. An additional portion of 4-amino-1-benzylpiperidine (25.0 g, 0.13 mol) was added and the reaction was stirred for another 30 min. The layers were separated, and the aqueous layer was re-extracted with DCM (2 \times 2 L). The total volume of the combined organics containing the title imine **11** was 13 L. A volume of 11.3 L (87% of total, ~ 4.2 mol based on amine) was used as the DCM solution in the next step. The remaining 1.7 L was evaporated to afford **11** (315 g, $\sim 85\%$ purity, ~ 0.6 mol) as a tan solid. ^1H NMR (CDCl_3) δ 8.61 (d, $J = 5.1$ Hz, 1H), 8.27 (br s, 2H), 7.59 (d, $J = 5.3$ Hz, 1H), 7.25–7.46 (m, 10H), 5.26 (m, 2H), 3.58 (br s, 2H), 3.33–3.43 (m, 1H), 2.91–2.99 (m, 2H), 2.10–2.25 (m, 2H), 1.82–1.95 (m, 2H), 1.63–1.82 (m, 2H).



Step 3: Preparation of Benzyl 4-[[1-(1-Benzylpiperidin-4-yl)-4-(4-fluorophenyl)-1H-imidazol-5-yl]pyrimidin-2-ylcarbamate (12). 1-Fluoro-4-[[isocyanato(tosyl)methyl]benzene (1176 g, 4.06 mol) and 20% aq. K_2CO_3 (5.6 L, 8.1 mol) were added to a solution of imine **11** (11 L, ~ 4 mol) in DCM at 20 °C, and the mixture was stirred at 25 °C overnight. Additional **11** (300 mL of DCM solution, ~ 0.1 mol) and 400 g of K_2CO_3 were added at this point, and the mixture was heated at 30 °C and stirred again overnight. The organic phase was separated and the aqueous layer was re-extracted with DCM (2 \times 2 L). The combined organics were dried over MgSO_4 (400 g) and Darco (80 g) for 45 min, filtered through a pad of Celite and Supercel, and washed with DCM. The filtrate was concentrated to a ~ 6 L volume, and then hexane (4 L) was added. The resulting solids were filtered, washed with 3 L 3:1 hexane/DCM followed by 2 L hexane, and dried at 45 °C under vacuum to afford the title compound **12** (1413 g, 2.51 mol, 62%) as an off-white solid. ^1H NMR ($\text{DMSO}-d_6$) δ 10.73 (s, 1H), 8.50 (d, $J = 5.1$ Hz, 1H), 8.14 (s, 1H), 7.21–7.47 (m, 12H), 7.12–7.18 (m, 2H), 6.86 (d, $J = 5.1$ Hz, 1H), 5.20 (s, 2H), 4.85–4.93 (m, 1H), 3.44 (s, 2H), 2.82 (br d, $J = 10.9$ Hz, 2H), 2.01–2.09 (m, 2H), 1.89–1.98 (m, 4H). ^{13}C NMR ($\text{DMSO}-d_6$) δ 161.5 (d, $J_{\text{C-F}} = 244.4$ Hz), 158.6, 158.2, 157.9, 151.8, 141.2, 138.5, 137.3, 136.6, 130.9 (d, $J_{\text{C-F}} = 2.9$ Hz), 129.9 (d, $J_{\text{C-F}} = 8.1$ Hz), 128.8, 128.4, 128.1, 129.0, 127.9, 126.9, 124.0, 116.4, 115.2 (d, $J_{\text{C-F}} = 21.4$ Hz), 65.8, 61.9, 53.1, 52.0, 32.8. HRMS m/z , calcd MH^+ 563.2571, observed 563.2563.



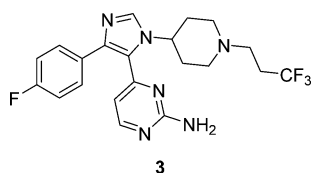
Step 4: Preparation of 4-[4-(4-Fluorophenyl)-1-(piperidin-4-yl)-1H-imidazol-5-yl]pyrimidin-2-amine (2). A mixture of **12** (800 g, 1.42 mol), 20 wt % $\text{Pd}(\text{OH})_2/\text{C}$ (50% H_2O , 60 g, 3 mol %), and

methanol (6.4 L) was hydrogenated at 60 psi at 40 °C for 18 h. The mixture was filtered through Solka-Floc, and the filtrate was concentrated to yield a thick slurry. Cyclohexane (2 L) was added, and the solids were filtered and washed with cyclohexane. This material was combined with product from a second run (from 825 g starting material) and dried at 45 °C under vacuum to afford **1** (883 g, 2.61 mol, 90%) as a white solid, which was suitable for use in the alkylations and reductive aminations. The HCl salt, prepared in EtOH and recrystallized from EtOH/water, had mp 193–197 °C (dec). ¹H NMR (MeOH-*d*₄) δ 8.12 (d, *J* = 5.1 Hz, 1H), 8.07 (s, 1H), 7.39–7.45 (m, 2H), 7.07–7.12 (m, 2H), 6.40 (d, *J* = 5.1 Hz, 1H), 4.99 (tt, *J* = 12.1, 3.9 Hz, 1H), 3.53–3.60 (m, 2H), 3.21 (ddd, *J* = 13.3, 13.3, 3.2 Hz, 2H), 2.45–2.53 (m, 2H), 2.24 (dddd, *J* = 13.2, 13.2, 13.2, 3.9 Hz, 2H). ¹³C NMR (MeOH-*d*₄) δ 165.1, 164.2 (d, *J*_{C-F} = 246.7 Hz), 159.9, 159.7, 142.8, 137.5, 131.7 (d, *J*_{C-F} = 8.1 Hz), 131.5 (d, *J*_{C-F} = 3.7 Hz), 126.4, 116.5 (d, *J*_{C-F} = 22.1 Hz), 112.8, 52.9, 45.0, 31.4. HRMS *m/z*, calcd MH⁺ 339.1733, observed 339.1731.



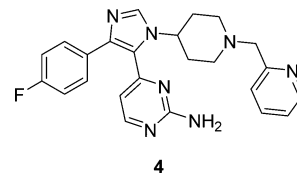
4-[(4-Fluorophenyl)-1-[1-(1,2-oxazol-3-ylmethyl)piperidin-4-yl]-1H-imidazol-5-yl]pyrimidin-2-amine (6). Isoxazole-3-carbaldehyde (25.8 g, 265.7 mmol) and **2** (64.2 g, 189.8 mmol) were slurried in THF (1.2 L). After the reaction mixture had been stirred for 15 min, sodium triacetoxyborohydride (120.7 g, 540 mmol) was added and the mixture was cooled to maintain the temperature below 37 °C. After 1.5 h of stirring, the reaction was slowly quenched with aq. NaHCO₃ (1.4 L H₂O/210 g NaHCO₃) and then diluted with 2-MeTHF (2 L). The layers were separated, the aqueous layer was re-extracted with 2-MeTHF (500 mL), and the combined organics were dried over Na₂SO₄, filtered, and concentrated to afford a pale oil. This crude oil was diluted with MeOH (200 mL), and the slurry was spun on the rotary evaporator at 55 °C for 1 h as the product crystallized out. The suspension was diluted with MTBE (100 mL) and cooled to rt; the solid was collected by filtration. The filter cake was washed with MTBE and was dried in vacuo at 40 °C to afford 63.8 g of the title compound as a granular white solid. The filtrate was concentrated and purified by chromatography using 2–8% MeOH/DCM + 1% NH₄OH to yield another 4.4 g of material; total yield 68.2 g (85%). This material was recrystallized from DCM/MeOH to provide analytically pure material. ¹H NMR (CDCl₃) δ 8.37 (d, *J* = 1.6 Hz, 1H), 8.16 (d, *J* = 5.1 Hz, 1H), 7.75 (s, 1H), 7.41–7.46 (m, 2H), 6.95–7.01 (m, 2H), 6.48 (d, *J* = 5.1 Hz, 1H), 6.39 (d, *J* = 1.6 Hz, 1H), 5.35 (br s, 2H), 4.53 (tt, *J* = 11.7, 4.3 Hz, 1H), 3.67 (s, 2H), 2.99 (br d, *J* = 12.1 Hz, 2H), 2.08–2.21 (m, 4H), 2.00 (dddd, *J* = 11.7, 11.7, 11.7, 3.5 Hz, 2H). ¹³C NMR (CDCl₃) δ 162.2 (d, *J*_{C-F} = 246.7 Hz), 163.0, 160.0, 159.0, 158.5, 158.4, 141.8, 135.7, 130.3 (d, *J*_{C-F} = 2.9 Hz), 129.8 (d, *J*_{C-F} = 8.1 Hz), 124.7, 115.2 (d, *J*_{C-F} = 22.1 Hz), 112.7, 104.4, 53.6, 52.8, 52.7, 33.2. HRMS *m/z*, calcd MH⁺ 420.1948, observed 420.1943.

The following compounds were prepared by reductive amination in similar fashion:

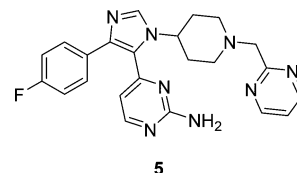


4-[(4-Fluorophenyl)-1-[1-(3,3,3-trifluoropropyl)piperidin-4-yl]-1H-imidazol-5-yl]pyrimidin-2-amine (3). Using 3,3,3-trifluoropropanal in place of isoxazole-3-carbaldehyde, isolated as a white solid. ¹H NMR (MeOH-*d*₄) δ 8.13 (d, *J* = 5.3 Hz, 1H), 8.03 (s, 1H), 7.38–7.44 (m, 2H), 7.04–7.10 (m, 2H), 6.41 (d, *J* = 5.1 Hz, 1H), 4.63 (tt, *J* = 11.7, 3.9 Hz, 1H), 3.06 (br d, *J* = 11.9 Hz, 2H), 2.65–2.69 (m, 2H), 2.36–2.49 (m, 2H), 2.11–2.24 (m, 4H), 2.03 (dddd, *J* = 11.9, 11.9, 11.9, 3.5 Hz, 2H). ¹³C NMR (CDCl₃) δ 165.1, 164.1 (d, *J*_{C-F} = 245.9

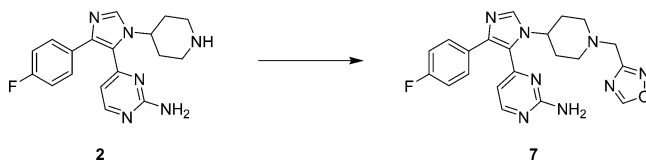
Hz), 160.4, 159.7, 124.2, 137.5, 131.6 (d, *J*_{C-F} = 3.7 Hz), 131.5 (d, *J*_{C-F} = 8.1 Hz), 128.4 (q, *J*_{C-F} = 275.4 Hz), 126.9, 116.5 (d, *J*_{C-F} = 22.1 Hz), 113.0, 55.5, 53.8, 51.6 (q, *J*_{C-F} = 3.7 Hz), 34.1, 32.6 (q, *J*_{C-F} = 28.0 Hz). HRMS *m/z*, calcd MH⁺ 435.1920, observed 435.1915.



4-[(4-Fluorophenyl)-1-[1-(pyridin-2-ylmethyl)piperidin-4-yl]-1H-imidazol-5-yl]pyrimidin-2-amine (4). Using picolinaldehyde in place of isoxazole-3-carbaldehyde, isolated as a white solid. ¹H NMR (MeOH-*d*₄) δ 8.49 (ddd, *J* = 5.1, 1.8, 1.0 Hz, 1H), 8.13 (d, *J* = 5.1 Hz, 1H), 7.83 (ddd, *J* = 7.8, 7.8, 1.8 Hz, 1H), 7.57 (br d, *J* = 8.0 Hz, 1H), 7.38–7.43 (m, 2H), 7.33 (ddd, *J* = 7.4, 4.9, 1.2 Hz, 1H), 7.04–7.10 (m, 2H), 6.40 (d, *J* = 5.3 Hz, 1H), 4.62 (tt, *J* = 10.2, 5.5 Hz, 1H), 3.70 (s, 2H), 3.02 (br d, *J* = 12.1 Hz, 2H), 2.26 (ddd, *J* = 11.3, 11.3, 3.2 Hz, 2H), 2.04–2.14 (m, 4H). ¹³C NMR (MeOH-*d*₄) δ 165.1, 164.0 (d, *J*_{C-F} = 246.5 Hz), 160.4, 159.7, 159.5, 149.8, 142.2, 138.9, 137.6, 131.6 (d, *J*_{C-F} = 3.7 Hz), 131.5 (d, *J*_{C-F} = 8.1 Hz), 126.9, 125.3, 124.1, 116.4 (d, *J*_{C-F} = 22.1 Hz), 113.0, 64.6, 55.6, 54.1, 34.2. HRMS *m/z*, calcd MH⁺ 430.2155, observed 430.2152.



4-[(4-Fluorophenyl)-1-[1-(pyrimidin-2-ylmethyl)piperidin-4-yl]-1H-imidazol-5-yl]pyrimidin-2-amine (5). 2-(Chloromethyl)pyrimidine (85.4 mg, 0.75 mmol), cesium carbonate (0.31 mL, 2.98 mmol) and **2** (252 mg, 0.75 mmol) in 3:1 THF/H₂O (4 mL) were heated at 70 °C for 18 h. EtOAc (25 mL) was added and the mixture was washed with water and with brine, dried over MgSO₄ and concentrated to yield a white solid. Chromatography with 5%–20% MeOH/EtOAc yielded a gummy white solid, which was washed with EtOAc to give 120 mg (46%) of the title compound as a white solid. Proton NMR showed desired product incorporating ~15% EtOAc that could not be removed by drying under high vacuum up to 100 °C. An analytically pure sample was prepared by first making the HCl salt: 1.1 equiv HCl/diethyl ether (1 M) was added to an EtOAc solution of free base. Concentration gave a gummy yellow salt that was then stirred with 5 mL sat. aq. NaHCO₃, resulting in a light tan oily precipitate. Addition of ~0.5 mL of MeOH and stirring yielded a light tan-colored solid, which was collected and dried under high vacuum at 100 °C to yield 84 mg of analytically pure, solvent-free material. ¹H NMR (MeOH-*d*₄) δ 8.80 (d, *J* = 5.1 Hz, 2H), 8.13 (d, *J* = 5.3 Hz, 1H), 8.04 (s, 1H), 7.38–7.43 (m, 3H), 7.04–7.10 (m, 2H), 6.40 (d, *J* = 5.1 Hz, 1H), 4.57–4.68 (m, 1H), 3.84 (s, 2H), 3.08 (br d, *J* = 12.1 Hz, 2H), 2.28–2.38 (m, 2H), 2.05–2.17 (m, 4H). ¹³C NMR (MeOH-*d*₄) δ 168.4, 165.1, 164.0 (d, *J*_{C-F} = 245.9 Hz), 160.4, 159.7, 158.8, 142.1, 137.6, 131.6 (d, *J*_{C-F} = 3.0 Hz), 131.5 (d, *J*_{C-F} = 8.1 Hz), 126.9, 121.4, 116.4 (d, *J*_{C-F} = 22.1 Hz), 113.0, 65.2, 55.4, 54.2, 34.0. HRMS *m/z*, calcd MH⁺ 431.2108, observed 431.2099.



4-[(4-Fluorophenyl)-1-[1-(1,2,4-oxadiazol-3-ylmethyl)piperidin-4-yl]-1H-imidazol-5-yl]pyrimidin-2-amine (7). 3-(Chloromethyl)-1,2,4-oxadiazole (144 mg, 1.22 mmol) was added to a slurry of **2** (300 mg, 0.887 mmol) and triethylamine (0.37 mL, 2.66 mmol) in

Table 3. Mouse Circadian Rhythm Test Study Designs

study	doses (mg/kg)	days of dosing	baseline condition	dosing condition	dosing time	postdosing condition
1	3.2, 10, 17.8	14	LD	LD	ZT11	DD

DCM (10 mL). THF (10 mL) was added to fully dissolve all solids. The resulting mixture was stirred at rt for 1 h and then refluxed for 22.5 h. The mixture was cooled and a white solid was filtered off. This solid was shown to be the HCl salt of **2** by ^1H NMR. The filtrate was then concentrated, redissolved in EtOAc and washed with water and with brine, dried over MgSO_4 , filtered, and concentrated onto silica gel. Flash chromatography using EtOAc and 5% MeOH/EtOAc afforded 95 mg (25%) of the title compound as a white solid. A portion was recrystallized from MeOH/EtOAc to provide an analytical sample: ^1H NMR (MeOH- d_4) δ 9.24 (s, 1H), 8.13 (d, $J = 5.5$ Hz, 1H), 8.03 (s, 1H), 7.38–7.43 (m, 2H), 7.03–7.09 (m, 2H), 6.40 (d, $J = 5.1$ Hz, 1H), 4.59 (tt, $J = 11.3, 4.7$ Hz, 1H), 3.82 (s, 2H), 3.10 (br d, $J = 11.7$ Hz, 2H), 2.31–2.38 (m, 2H), 2.05–2.15 (m, 4H). ^{13}C NMR (CDCl_3) δ 167.9, 166.5 (d, $J_{\text{C-F}} = 254.0$ Hz), 165.1, 162.8, 160.4, 159.7, 142.2, 137.6, 131.6 (d, $J_{\text{C-F}} = 3.7$ Hz), 131.5 (d, $J_{\text{C-F}} = 8.1$ Hz), 126.9, 116.4 (d, $J_{\text{C-F}} = 22.1$ Hz), 113.0, 55.3, 53.8, 53.1, 34.1. HRMS m/z , calcd MH^+ 421.1901, observed 421.1896.

In Vitro Materials. OptiMEM (Gibco 31985), Dulbecco's modified Eagle's medium (Gibco 11995), fetal bovine serum (Sigma F-4135), TrypLE Express (Gibco 12605), Lipofectamine 2000 reagent (Invitrogen), mouse PER3-GFP in pd2EGFP-N1 vector (in-house reagent), human CK1 in pcDNA4/hisA vector (Lamda Biotech, Inc., custom order), Greiner Bio-one Cellcoat PDL plates, μ -clear, no.781946, PBS 10 \times (Biosolutions BIO460), PBS 1 \times (Sigma D8537), paraformaldehyde (Electron Microscopy Sciences 15710-S), normal goat serum (Vector Laboratories V0505), Triton X 88 (Sigma T8787), Hoechst 33342 (Invitrogen H3570), Alexa Fluor 488 goat anti-rabbit IgG (H+L), 2 mg/mL (Invitrogen A11008), anti-GFP rabbit IgG fraction, 2 mg/mL (Invitrogen A11122), plate seals (PerkinElmer 6005189), and DMSO (JT Baker 9224-0).

Kinase Assay. The CK1 δ kinase assay was performed in a 40 μL final volume in buffer containing 50 mM Tris, pH 7.5, 10 mM MgCl_2 , 1 mM dithiothreitol, 100 $\mu\text{g}/\text{mL}$ BSA with 10 μM ATP, 2 nM CK1 δ wild-type, and 42 μM peptide substrate PLSRTLpSVASLPGL in the presence of 1 μL of CK1 δ inhibitor or 4% DMSO.³⁶ The reaction was incubated for 40 min at 25 $^\circ\text{C}$; detection was carried out as described for the Kinase-Glo assay (Promega).

Luminescent output was measured on the PerkinElmer EnVision plate reader (PerkinElmer, Waltham, MA). The CK1 ϵ kinase assay was performed in a 40 μL final volume in buffer containing 50 mM Tris, pH 7.5, 10 mM MgCl_2 , 1 mM dithiothreitol, 100 $\mu\text{g}/\text{mL}$ BSA with 10 μM ATP, 2.5 nM CK1 ϵ wild-type, and 42 μM peptide substrate PLSRTLpSVASLPGL in the presence of 1 μL of CK1 ϵ inhibitor or 4% DMSO.³⁶ The reaction was incubated for 70 min at 25 $^\circ\text{C}$; detection was carried out as described for the Kinase-Glo assay (Promega). Luminescent output was measured on the PerkinElmer EnVision plate reader (PerkinElmer, Waltham, MA).

CK1 WCA HCS Nuclear Translocation Assay. Cos7 cells were maintained at 37 $^\circ\text{C}$ in 5% CO_2 in Dulbecco's modified Eagle's medium (Gibco 11995) supplemented with 10% fetal bovine serum. Log-phase cells were dislodged with 5 min treatment of TrypLE Express (Gibco 12605), and viable cell count was determined with Cedex cell counter. Cells were diluted in DMEM medium to a density of 1.5×10^5 viable cells/mL in 2/3 of the final volume of final transfected cell mix. Cells were cotransfected with two plasmid DNAs, mouse Per3-GFP (green fluorescent protein) in pd2EGFP-N1 vector and human CK1 in pcDNA4/hisA vector (for CK1 ϵ at a ratio of 1:5 respectively; for CK1 δ at a ratio of 1:11 respectively), using Lipofectamine 2000 reagent (Invitrogen) according to the manufacturer's recommendations. The transfection mix contained approximately 0.83 $\mu\text{g}/\text{mL}$ DNA and 6 $\mu\text{L}/\text{mL}$ Lipofectamine 2000, in a total of 1/3 of the final transfection volume in Opti-MEM I medium (Invitrogen). After 20 min at rt, the cell mix was combined with the DNA transfection mix, per manufacturer instructions. Next, 50 μL of the transfected cell suspension was dispensed per well by multidrop

dispenser into Greiner 384-well Cellcoat (PDL) plates (Greiner # 781946). Compounds were solubilized in 100% DMSO and diluted with Opti-MEM I to a 4 \times concentration before addition to plated cells. After overnight exposure at 37 $^\circ\text{C}$ in a CO_2 incubator, cells were fixed by the addition of 12% paraformaldehyde (Electron Microscopy Sciences, Hatfield, PA) in phosphate-buffered saline (PBS) with 20% sucrose to a final concentration of 4%, and then the cells were incubated for 30 min at rt. Fixative was removed, and cells were washed with PBS and then stained with 0.4 $\mu\text{g}/\text{mL}$ Hoechst dye (Invitrogen) in blocking buffer containing 4% goat serum (Vector Laboratories s-1000) and 0.1% Triton X (Sigma T8787) for 1 h. Cells were washed again with PBS and stored at 4 $^\circ\text{C}$ in PBS or scanned immediately with the Cellomics ArrayScan VTI system. CK1 δ/ϵ -dependent nuclear localization of the GFP-tagged mPer3 protein was quantitated using the Cellomics ArrayScan VTI system utilizing the Cytoplasm to Nucleus translocation bioapplication to calculate the Nuclear-Cytoplasmic Intensity difference. Inhibitors of CK1 δ/ϵ were tested across a dose response curve to evaluate their ability to inhibit mPer3-GFP translocation to the nucleus. Cells with a total intensity of mPER3:GFP expression equal to or greater than 20 000 are included in the analysis.

In Vivo Methods and Materials: Mouse Circadian Rhythm Test. All procedures involving animals were conducted with approval of the Pfizer Institutional Animal Care and Use Committee. The mouse strain used in the mouse circadian rhythm (MCR) assay was C57BL/6J (Jackson Laboratory, Bar Harbor, ME), a popular inbred strain for circadian studies. Males were used to avoid any effect of estrus on circadian rhythm. Mice were surgically implanted with intraperitoneal transmitters (Data Sciences International, St. Paul, MN) according to manufacturer's guidelines and using strict aseptic technique. Appropriate levels of anesthesia and analgesia were maintained throughout the procedure and during recovery. Approximately 1 week after surgery, wound clips were removed and animals were placed in running wheel cages and into isolation boxes. The mice were housed one per cage, with four cages in each isolation box. The baseline lighting schedule was 12 h of lights-on followed by 12 h of lights-off (LD12:12). Mice were housed in LD12:12 for 10–14 days prior to each study to ensure stable rhythms. Body temperature and gross motor activity data were recorded for each animal, with temperature data being used for analysis. The daily rise in body temperature was used as the activity onset for each day. Baseline data was reviewed for quality and to meet exclusion criteria. Animals were excluded if their baseline tau, or length of their day in hours, was <23.90 or >24.10 h. Animals were also excluded if the quality of their data was insufficient to allow for reliable determination of activity onsets. Exclusions were determined prior to randomization of treatment groups.

Treatment groups consisted of 4–8 mice with each isolation box containing mice from different groups. Studies were conducted with 3–7 treatment groups including a vehicle group. The vehicle used was 20% w/v sulfobutylether- β -cyclodextrin (SBECD) in sterile water. Compound **6** was dissolved in this vehicle with 2 mol equiv of hydrochloric acid at a dosing volume of 10 mL per kilogram body weight. All dosing was done subcutaneously at a frequency of once per day with injection sites alternated daily. For some studies, the animals were housed in LD12:12 throughout dosing. In these studies, the specific dosing time was 1 h before lights-off. This time is referred to as zeitgeber time 11 (ZT11). A zeitgeber is a synchronizing agent capable of entraining the circadian clock; in this case, the zeitgeber is light. Dosing was done at circadian time 11 (CT11). For a nocturnal animal in DD, this time is defined as 1 h before activity onset. Since dosing began 1 day after the animals were in LD12:12, CT11 was considered to be equivalent to ZT11. Duration of dosing was 14 days. After the completion of dosing, mice were housed in the conditions outlined in Table 3. They were monitored for at least 7 days postdosing. Data was

recorded using DataQuest software (Data Sciences International, St. Paul, MN) in 5 min bins. Text files were then converted to actograms and analyzed using ClockLab 2.61 (Actimetrics, Wilmette, IL) running on Matlab R2007b (The MathWorks Inc., Natick, MA).

Phase shift was the parameter by which the efficacy of **6** was measured. It is reported in hours. A positive value indicates a phase advance from baseline, whereas a negative value indicates a phase delay. Phase shift was calculated for each animal in ClockLab by denoting the onset of the daily rise in body temperature associated with increased activity during the lights-out phase. This was done for the baseline, dosing, and postdosing periods. Using ClockLab, regression lines were drawn through these onsets for the baseline and postdosing periods separately, and then the temporal differences between these regression lines represented the phase shift. For the 14 day studies where the animals were dosed in LD and remained in LD after the completion of dosing, the phase shift was calculated for the last day of dosing. In addition to phase shift, other parameters that were analyzed included baseline tau (also referred to as pretau) and postdosing tau (also referred to as post-tau). ClockLab calculates tau when regression lines are drawn through activity onsets. For baseline tau, this was done as further insurance, in addition to the exclusion criteria mentioned above, that there was no bias in the phase shift measurement as this is partially dependent on baseline tau. For postdosing tau, this was done to detect any differences in the endogenous circadian rhythms of the mice, which may influence response to compound. This is particularly useful when DD was used as the postdosing condition. For study 1, results were analyzed using ANOVA within the electronic notebook environment (ID Business Solutions LTD, Guildford, U.K.) with Dunnett's multiple comparison test. Compound **6** significantly phase-delayed mice after dosing in LD for 14 days with 17.8 and 10 mg/kg. The same dosing conditions for 3.2 mg/kg did not result in significant phase shifts. There were no significant differences between treatment groups for baseline tau or postdosing tau.

In Vivo Methods and Materials: Cynomolgus Monkey Circadian Rhythm Test. All procedures involving animals were conducted with approval of the Pfizer Institutional Animal Care and Use Committee and compliant with the regulations and standards of the Animal Welfare Act (9CFR2, 9CFR3). Animals: Eight 4- to 5-year-old male Mauritian cynomolgus macaques SPF for CHV-1, SRV 1, 2, and 5, STLV1, and SIV were used for all studies. Animals were pair-housed, chair-trained, and fitted with collar-mounted Actical monitors (Philips Respironics). The Actical device is an omnidirectional accelerometer that generates quantitative measurements of activity for up to 45 days continuously. Animals were acclimated for 2 weeks in a room with 12:45/11:15 light/dark cycles with a 45 min ramping period to full lights on/off as simulated dawn/dusk. The direct light intensity in the room was 1300 Lux measured 1 m from the floor in the middle of the room. Animals were chair-restrained for drug administration and data downloads from the Actical monitors.

Drug Preparation and Administration. Compound **6** was dissolved in acidified, aqueous, 20% w/v sulfobutylether- β -cyclodextrin (SBECD) final pH 3.5. The vehicle was prepared in sterile water. Drug and vehicle were prepared 1–2 h prior to administration and dosed orally at a volume of 2.0 mL per kilogram of body weight.

Phase Shift Induction. A crossover design was used for all experiments. Prior to each study, animal pairs were randomized into drug and vehicle groups. Following at least 7 days of stable entrainment in their home cage, animals were chaired and dosed for 3 consecutive days at 16:30. After a washout period of 7–10 days, animals were re-entrained, treatment group crossed-over, and dosed for 3 consecutive days at 16:30.

Data Analysis. Actigrams and circadian data were generated using Clocklab 2.61 (Actimetrics Wilmette, IL) running on Matlab R2007b (The MathWorks, Inc., Natick, MA). Activity onset was used to determine phase shifts from analysis of individual actigrams for each animal. The Clocklab algorithm for determining activity onset was employed using a 6 h period of inactivity followed by a 6 h period of high activity setting. Activity onset is taken as the time of day that best approximates this pattern. Phase shifts were calculated from least-

squares fits of activity onsets. Data was analyzed by repeated measure ANOVA and Bonferroni's Multiple Comparison Test using GraphPad Prism 5.0 (GraphPad Software, San Diego, CA).

In Vivo Methods and Materials: Fentanyl Self-Administration Test. **Drugs.** Fentanyl citrate salt (Sigma-Aldrich, St. Louis, MO) was dissolved in 0.9% saline solution. Compound **6** was formulated in 20% sulfobutylether- β -cyclodextrin (SBECD)/1 N hydrochloric acid (HCl). All drug concentrations and doses refer to the active moiety.

Surgery. Sprague–Dawley rats (Charles River Laboratories, Durham, NC) were implanted with jugular vein catheters (JVC) with modifications to previously described methods.³⁷ Briefly, on the day of surgery, anti-inflammatory and antibiotic treatment was provided (Carprofen, 5 mg/kg; enrofloxacin, 2.25 mg/kg; s.c.). Rats were anaesthetized with isoflurane (2.5–3.5% in 100% oxygen), and a JVC (modified IVSAP40 catheter: CamCaths, Cambridge, U.K.), previously sterilized by exposure to ethylene oxide gas, was implanted. The proximal end was placed at the right atrium, entering at the right jugular vein, while the distal end was passed over the right shoulder and exited dorsally, between the scapulae. Carprofen (5 mg/kg) and enrofloxacin (2.25 mg/kg) were given subcutaneously for at least 2 days postoperatively. A minimum of 7 days postsurgical recovery was allowed prior to use in experiments. Catheter patency was maintained with daily i.v. infusions of 0.1 mL of heparinized (50 units/mL) sterile 0.9% saline. When rats were not used for periods longer than 48 h, catheters were locked with heparinized (50 units/mL) dextrose. Catheter patency was assessed by injection of 0.1 mL of propofol. Rats were food-restricted to ~22 g of rodent diet per day, and fed at the end of each day after operant sessions had completed.

Apparatus. Self-administration training and testing occurred in operant chambers (ENV-008CT; Med-Associates, St. Albans, VT) individually located within sound-attenuating cubicles, which were ventilated with an exhaust fan that also served to mask external noise. Two retractable response levers (ENV-112CM, Med-Associates) were located on one wall of the operant chamber, 12 cm apart and 6 cm from the grid floor. A cue light (ENV-221M, Med-Associates) was located approximately 4 cm above each lever. On the wall opposite to the response levers was positioned a house light (ENV 215M, Med-Associates) and response feedback clicker module (ENV-135M). Drug was infused by a fixed rate syringe pump (PHM100, Med-Associates), located outside the sound attenuating cubicle, via plastic tubing (polyethylene, SAI Infusion Technologies, Lake Villa, IL) connected from the infusion syringe to a stainless steel single channel swivel (model 375/22: Instech Laboratories, Plymouth Meeting, PA) mounted directly above the operant chamber on a counterbalanced lever arm (PHM-110, Med-Associates). A further length of tubing, shielded by a metal spring tether, connected from the swivel to the external guide cannulae of the implanted JVC. Med-PC IV software (Med-Associates) was used to control operant chambers and record data.

Self-Administration Training Procedure. Methods were adapted from O'Connor et al.³⁷ Rats were placed into the operant chambers and self-administration sessions commenced with an automatic infusion designed to fill the JVC with drug. The house light was then illuminated and both response levers were extended into the operant chamber. Responding on one lever (the active lever) under a fixed ratio schedule resulted in fentanyl delivery, followed by a timeout period of 20 s, during which time the cue lights located above the levers were flashed at a rate of 0.5 Hz and a clicking sound was presented at the same time as the light cue. Further responding during this timeout period on the active lever was recorded but had no scheduled consequence. Responding on the alternative lever (the inactive lever) was recorded throughout the experimental session but had no scheduled outcome. Active and inactive levers were randomly assigned to each rat prior to the first session and did not change throughout the study. The unit dose of drug available was determined by the unit volume per infusion (as determined by the duration of the infusion) and adjusted for the weight of the rat. The duration of infusion was maintained at between 1 and 3 s. All experiments started within 1 h prior to lights out, between 8:00 and 10:00 AM, up to 5 days per week. All sessions were 1.5 h in duration.

Effects of 6 on Reinstatement of Fentanyl-Seeking. Twenty-two rats were trained to respond for fentanyl (3 $\mu\text{g}/\text{kg}/\text{infusion}$) under a FR5 schedule of reinforcement (i.e., five responses on the active lever resulted in a single infusion of fentanyl). When rats were demonstrating stable self-administration of fentanyl under an FR5 schedule (as defined by $\leq 20\%$ variation in the number of infusions obtained during two consecutive sessions), responding was extinguished by removing the contingency between the response and fentanyl delivery. In addition, cues associated with the infusion were also removed, including the flashing cue lights, clicking sound, the sound of the syringe pump, and the infusion itself. Following a minimum of five extinction sessions, and the demonstration of extinction (defined as a decrease in active lever responses to $< 30\%$ of the mean number of responses made during the final two sessions of fentanyl responding), reinstatement sessions began. Reinstatement test sessions consisted of a fentanyl prime (0.045 mg/kg) given 5 minutes prior to the start of the test session. During the reinstatement session, active lever presses resulted in presentation of the fentanyl-associated cues for 6 seconds, however no fentanyl was infused. Following each reinstatement session, rats were given a minimum of two extinction sessions where stability criteria must be met, prior to the next session. To determine the effect of 6 on reinstatement of fentanyl-seeking behavior, doses of 0, 0.5, 1.5, 5, 15, and 50 mg/kg were selected. Compound 6 was administered 30 min prior to all reinstatement tests. The order of 6 dose presentation was counterbalanced.

Analysis. For reinstatement tests, the baseline was defined as the average response on the 2 days preceding a reinstatement test, while the test was the number of responses on the reinstatement test session. Data from animals that did not reinstate under vehicle conditions (i.e., exhibited less active lever presses on test compared to baseline) and outliers (i.e., exhibited active lever presses greater than three standard deviations of the mean on vehicle) were excluded for each reinstatement condition.

For reinstatement tests, statistical analysis was performed using two-way repeated measures analysis of variance (ANOVA), with session (baseline vs test) and dose as factors for comparing responses (active and inactive lever presses) at baseline (i.e., the average of response rates during the sessions immediately preceding reinstatement sessions) with those during test reinstatement sessions. If a significant interaction or main-effect of dose was then observed, posthoc comparisons were made between responses following each dose of drug and vehicle, using Dunnett's test.

The significance level for all statistical tests was set at 0.05. All statistical analysis was performed using Statistica version 12.0 (StatSoft, Inc. 2014; STATISTICA (data analysis software system), version 12.0. www.statsoft.com).

Exposure Response Analysis. The effect of reinstatement prevention was quantified with the following equation:

$$\begin{aligned} & \% \text{ relapse prevention} \\ & = 100 \times \frac{(\text{VEH}_{\text{test}} - \text{VEH}_{\text{base}}) - (\text{TRT}_{\text{test}} - \text{TRT}_{\text{base}})}{\text{VEH}_{\text{test}} - \text{VEH}_{\text{base}}} \end{aligned}$$

where VEH_{test} and TRT_{test} represents lever presses under combined cue- and fentanyl prime-induced reinstatement test with vehicle and treatment group, respectively; VEH_{base} and TRT_{base} represents lever presses under baseline condition with vehicle and treatment group, respectively.

An E_{max} model was implemented to estimate potency in this model.

$$\% \text{ relapse prevention} = \frac{C_{\text{b,u}} \times 100}{C_{\text{b,u}} + \text{EC}_{50}}$$

where $C_{\text{b,u}}$ represents average free brain exposure from satellite animals and EC_{50} represents exposure required to elicit 50% prevention from relapse. Model fitting was performed using R 3.1.0.

■ ASSOCIATED CONTENT

§ Supporting Information

Table 1s: Mouse circadian rhythm results. Table 2s: Individual mouse circadian rhythm data. Table 3s: Individual monkey circadian rhythm data. Table 4s: Individual animals for reinstatement (baseline and test). Figure 1s: Effects of 6 on reinstatement of fentanyl-seeking behavior in the rat reinstatement model. This material is available free of charge via the Internet at <http://pubs.acs.org>.

Accession Codes

All coordinates have been deposited in the PDB with accession codes 4TN6 (6).

■ AUTHOR INFORMATION

Corresponding Author

*Tel: 857-225-2840. Fax 860-686-6052. E-mail: travis.t.wager@pfizer.com.

Author Contributions

T.T.W., M.M., G.D., A.D., C.C., D.H., and A.M. designed the experiment. R.Y.C., J.B., D.R., H.B., T.B. J.K., and A.R. performed the experiment. R.Y.C., J.B., K.F., S.L., J.O., B.S., and A.R. contributed to reagents and other resources. T.T.W., S.M., J.K., J.O., A.D., C.C., M.M., G.D., B.S., K.W., and D.H. performed data analyses. T.T.W., S.M. T.B., C.C. M.M., G.D. K.W., and D.H. wrote the manuscript.

Notes

PF-05006739 is now commercially available from Sigma-Aldrich (catalog # PZ-0246).

The authors declare no competing financial interest.

■ ACKNOWLEDGMENTS

The authors thank Jessica Adams for compound screening, Kristin Rockwell for HTS screening, and Mark Tibbets for cell culture support for the WC assay. The authors thank Nandini Patel for her analysis of the off-target pharmacology and generation of heat map table. The authors also thank Katherine Brightly for her insightful comments on this manuscript.

■ ABBREVIATIONS

ADME, absorption, distribution, metabolism and excretion; CPP, condition place preference; AUC, area under the curve; C_{aver} average concentration; C_{eff} efficacious concentration; C_{max} maximum concentration; $\text{CKI}\delta$, casein kinase 1 delta; $\text{CKI}\epsilon$, casein kinase 1 epsilon; CNS, central nervous system; DARPP-32, dopamine cAMP-regulated neuronal phosphoprotein; GFP, green fluorescent protein; HBD, hydrogen bond donor; HLM, human liver microsomes; MDR, multidrug resistance; MPO, multiparameter optimization; P-gp, P-glycoprotein; PER, PERIOD gene; SCN, suprachiasmatic nucleus; SAR, structure–activity relationship; SBDD, structure-based drug design; WCA, whole-cell assay

■ REFERENCES

- (1) Degenhardt, L., Whiteford, H. A., Ferrari, A. J., Baxter, A. J., Charlson, F. J., Hall, W. D., Freedman, G., Burstein, R., Johns, N., Engell, R. E., Flaxman, A., Murray, C. J. L., and Vos, T. (2013) Global burden of disease attributable to illicit drug use and dependence: Findings from the Global Burden of Disease Study. 2010. *Lancet* 382, 1564–1574.
- (2) Gallego, M., and Virshup, D. M. (2007) Post-translational modifications regulate the ticking of the circadian clock. *Nat. Rev. Mol. Cell Biol.* 8, 139–148.

- (3) Meng, Q.-J., Maywood, E. S., Bechtold, D. A., Lu, W.-Q., Li, J., Gibbs, J. E., Dupré, S. M., Chesham, J. E., Rajamohan, F., Knafels, J., Sneed, B., Zawadzke, L. E., Ohren, J. F., Walton, K. M., Wager, T. T., Hastings, M. H., and Loudon, A. S. I. (2010) Entrainment of disrupted circadian behavior through inhibition of casein kinase 1 (CK1) enzymes. *Proc. Natl. Acad. Sci. U.S.A.* 107, 15240–15245.
- (4) Ralph, M., and Menaker, M. (1988) A mutation of the circadian system in golden hamsters. *Science* 241, 1225–1227.
- (5) Lowrey, P. L., Shimomura, K., Antoch, M. P., Yamazaki, S., Zemenides, P. D., Ralph, M. R., Menaker, M., and Takahashi, J. S. (2000) Positional Syntenic Cloning and Functional Characterization of the Mammalian Circadian Mutation tau. *Science* 288, 483–491.
- (6) Xu, Y., Padiath, Q. S., Shapiro, R. E., Jones, C. R., Wu, S. C., Saigoh, N., Saigoh, K., Ptacek, L. J., and Fu, Y.-H. (2005) Functional consequences of a CK1[delta] mutation causing familial advanced sleep phase syndrome. *Nature* 434, 640–644.
- (7) Jones, C. R., Campbell, S. S., Zone, S. E., Cooper, F., DeSano, A., Murphy, P. J., Jones, B., Czajkowski, L., and Ptacek, L. J. (1999) Familial advanced sleep-phase syndrome: A short-period circadian rhythm variant in humans. *Nat. Med.* 5, 1062–1065.
- (8) Walton, K. M., Fisher, K., Rubitski, D., Marconi, M., Meng, Q.-J., Sladek, M., Adams, J., Bass, M., Chandrasekaran, R., Butler, T., Griffor, M., Rajamohan, F., Serpa, M., Chen, Y., Claffey, M., Hastings, M., Loudon, A., Maywood, E., Ohren, J., Doran, A., and Wager, T. T. (2009) Selective inhibition of casein kinase 1 ϵ minimally alters circadian clock period. *J. Pharmacol. Exp. Ther.* 330, 430–439.
- (9) Falcón, E., and McClung, C. A. (2009) A role for the circadian genes in drug addiction. *Neuropharmacology* 56 ((Suppl 1)), 91–96.
- (10) Abarca, C., Albrecht, U., and Spanagel, R. (2002) Cocaine sensitization and reward are under the influence of circadian genes and rhythm. *Proc. Natl. Acad. Sci. U.S.A.* 99, 9026–9030.
- (11) Spanagel, R., Pendyala, G., Abarca, C., Zghoul, T., Sanchis-Segura, C., Magnone, M. C., Lascorz, J., Depner, M., Holzberg, D., Soyka, M., Schreiber, S., Matsuda, F., Lathrop, M., Schumann, G., and Albrecht, U. (2005) The clock gene Per2 influences the glutamatergic system and modulates alcohol consumption. *Nat. Med.* 11, 35–42.
- (12) Perreau-Lenz, S., Vengeliene, V., Noori, H. R., Merlo-Pich, E. V., Corsi, M. A., Corti, C., and Spanagel, R. (2012) Inhibition of the Casein-Kinase-1-Epsilon/Delta Prevents Relapse-Like Alcohol Drinking. *Neuropsychopharmacology* 37, 2121–2131.
- (13) Svenningsson, P., Nairn, A. C., and Greengard, P. (2005) DARPP-32 mediates the actions of multiple drugs of abuse. *AAPS J.* 7, E353–E360.
- (14) Svenningsson, P., Nishi, A., Fisone, G., Girault, J.-A., Nairn, A. C., and Greengard, P. (2004) DARPP-32: An Integrator of Neurotransmission. *Annu. Rev. Pharmacol. Toxicol.* 44, 269–296.
- (15) Fernandez, É, S. R., Girault, J.-A., and Novère, N. L. (2006) DARPP-32 Is a Robust Integrator of Dopamine and Glutamate Signals. *PLoS Comput. Biol.* 2, e176.
- (16) Chergui, K., Svenningsson, P., and Greengard, P. (2005) Physiological Role for Casein Kinase 1 in Glutamatergic Synaptic Transmission. *J. Neurosci.* 25, 6601–6609.
- (17) Li, D., Herrera, S., Bubula, N., Nikitina, E., Palmer, A. A., Hanck, D. A., Loweth, J. A., and Vezina, P. (2011) Casein kinase 1 enables nucleus accumbens amphetamine-induced locomotion by regulating AMPA receptor phosphorylation. *J. Neurochem.* 118, 237–247.
- (18) Nairn, A. C., Svenningsson, P., Nishi, A., Fisone, G., Girault, J.-A., and Greengard, P. (2004) The role of DARPP-32 in the actions of drugs of abuse. *Neuropharmacology* 47 (Supplement 1), 14–23.
- (19) Mahajan, S. D., Aalinkeel, R., Reynolds, J. L., Nair, B. B., Sykes, D. E., Hu, Z., Bonoio, A., Ding, H., Prasad, P. N., and Schwartz, S. A. (2009) Therapeutic Targeting of “DARPP-32”: A Key Signaling Molecule in the Dopaminergic Pathway for the Treatment of Opiate Addiction. *International Review of Neurobiology* (Hari Shanker, S., Ed.), Chapter 8, pp 199–222, Academic Press, New York.
- (20) Bryant, C., Graham, M., Distler, M., Munoz, M., Li, D., Vezina, P., Sokoloff, G., and Palmer, A. (2009) A role for casein kinase 1 epsilon in the locomotor stimulant response to methamphetamine. *Psychopharmacology* 203, 703–711.
- (21) Bryant, C. D., Parker, C. C., Zhou, L., Olker, C., Chandrasekaran, R. Y., Wager, T. T., Bolivar, V. J., Loudon, A. S., Vitaterna, M. H., Turek, F. W., and Palmer, A. A. (2012) Csnk1e Is a Genetic Regulator of Sensitivity to Psychostimulants and Opioids. *Neuropsychopharmacology* 37, 1026–1035.
- (22) Mente, S., Arnold, E., Butler, T., Chakrapani, S., Chandrasekaran, R., Cherry, K., DiRico, K., Doran, A., Fisher, K., Galatsis, P., Green, M., Hayward, M., Humphrey, J., Knafels, J., Li, J., Liu, S., Marconi, M., McDonald, S., Ohren, J., Paradis, V., Sneed, B., Walton, K., and Wager, T. (2013) Ligand–Protein Interactions of Selective Casein Kinase 1 δ Inhibitors. *J. Med. Chem.* 56, 6819–6828.
- (23) Badura, L., Swanson, T., Adamowicz, W., Adams, J., Cianfrogna, J., and Fisher, K. (2007) An inhibitor of casein kinase I epsilon induces phase delays in circadian rhythms under free-running and entrained conditions. *J. Pharmacol. Exp. Ther.* 322, 730–738.
- (24) Wager, T. T., Chandrasekaran, R. Y., Hou, X., Troutman, M. D., Verhoest, P. R., Villalobos, A., and Will, Y. (2010) Defining Desirable Central Nervous System Drug Space through the Alignment of Molecular Properties, in Vitro ADME, and Safety Attributes. *ACS Chem. Neurosci.* 1, 420–434.
- (25) Wager, T. T., Hou, X., Verhoest, P. R., and Villalobos, A. (2010) Moving beyond rules: The development of a central nervous system multiparameter optimization (CNS MPO) approach to enable alignment of druglike properties. *ACS Chem. Neurosci.* 1, 435–449.
- (26) Mente, S., Doran, A., and Wager, T. T. (2012) Getting the MAX out of computational models: The prediction of unbound-brain and unbound-plasma maximum concentrations. *ACS Med. Chem. Lett.* 3, 515–519.
- (27) Wager, T. T., Kormos, B. L., Brady, J. T., Will, Y., Aleo, M. D., Stedman, D. B., Kuhn, M., and Chandrasekaran, R. Y. (2013) Improving the Odds of Success in Drug Discovery: Choosing the Best Compounds for in Vivo Toxicology Studies. *J. Med. Chem.* 56, 9771–9779.
- (28) Marchant, N. J., Li, X., and Shaham, Y. (2013) Recent developments in animal models of drug relapse. *Curr. Opin. Neurobiol.* 23, 675–683.
- (29) Morgan, P., Van Der Graaf, P. H., Arrowsmith, J., Feltner, D. E., Drummond, K. S., Wegner, C. D., and Street, S. D. A. (2012) Can the flow of medicines be improved? Fundamental pharmacokinetic and pharmacological principles toward improving Phase II survival. *Drug Discovery Today* 17, 419–424.
- (30) Ertl, P. (2008) Polar surface area. *Methods Princ. Med. Chem.* 37, 111–126.
- (31) Feng, B., Mills, J. B., Davidson, R. E., Mireles, R. J., Janiszewski, J. S., Troutman, M. D., and de Morais, S. M. (2008) In vitro P-glycoprotein assays to predict the in vivo interactions of P-glycoprotein with drugs in the central nervous system. *Drug Metab. Dispos.* 36, 268–275.
- (32) Hosea, N. A., Collard, W. T., Cole, S., Maurer, T. S., Fang, R. X., Jones, H., Kakar, S. M., Nakai, Y., Smith, B. J., Webster, R., and Beaumont, K. (2009) Prediction of human pharmacokinetics from preclinical information: comparative accuracy of quantitative prediction approaches. *J. Clin. Pharmacol.* 49, 513–533.
- (33) Gao, H., Yao, L., Mathieu, H. W., Zhang, Y., Maurer, T. S., Troutman, M. D., Scott, D. O., Ruggeri, R. B., and Lin, J. (2008) In silico modeling of nonspecific binding to human liver microsomes. *Drug Metab. Dispos.* 36, 2130–2135.
- (34) Newman, A. H., Beuming, T., Banala, A. K., Donthamsetti, P., Pongetti, K., LaBounty, A., Levy, B., Cao, J., Michino, M., Luedtke, R. R., Javitch, J. A., and Shi, L. (2012) Molecular determinants of selectivity and efficacy at the dopamine D3 receptor. *J. Med. Chem.* 55, 6689–6699.
- (35) Lu, Y., Kingsbury, C., Bohnstedt, A., Ohlmeyer, M., and Paradkar, V. (2008) 8-Substituted 2-(benzimidazolyl) purine derivatives as immunosuppressants and their preparation, pharmaceutical compositions and use in the treatment of immune diseases. Patent WO2008043019A1.

(36) Flotow, H., Graves, P. R., Wang, A. Q., Fiol, C. J., Roeske, R. W., and Roach, P. J. (1990) Phosphate groups as substrate determinants for casein kinase I action. *J. Biol. Chem.* 265, 14264–14269.

(37) O'Connor, E. C., Parker, D., Rollema, H., and Mead, A. N. (2010) The alpha4beta2 nicotinic acetylcholine-receptor partial agonist varenicline inhibits both nicotine self-administration following repeated dosing and reinstatement of nicotine seeking in rats. *Psychopharmacology (Berlin, Ger.)* 208, 365–376.